

## Article

# Active Control of Electromagnetically Induced Transparency Analogy in Spoof Surface Plasmon Polariton Waveguide

Xiaoqiang Su <sup>1,\*</sup>, Lijuan Dong <sup>1,\*</sup>, Jiajun He <sup>1</sup>, Yucong Huang <sup>1</sup>, Fusheng Deng <sup>1</sup>, Lifeng Liu <sup>1</sup>, Yunlong Shi <sup>1</sup>, Quan Xu <sup>2</sup> and Yanfeng Li <sup>2,\*</sup> 

<sup>1</sup> Institute of Solid State Physics and College of Physics and Electronic Science, Shanxi Province Key Laboratory of Microstructure Electromagnetic Functional Materials, Shanxi Datong University, Datong 037009, China

<sup>2</sup> Center for Terahertz Waves and College of Precision Instrument and Optoelectronics Engineering, Key Laboratory of Optoelectronic Information Technology (Ministry of Education of China), Tianjin University, Tianjin 300072, China

\* Correspondence: lijuan\_dong@sxdtu.edu.cn (L.D.); yanfengli@tju.edu.cn (Y.L.)

**Abstract:** Metamaterial analogues of electromagnetically induced transparency (EIT) enable a unique avenue to endow a coupled resonator system with quantum interference behavior, exhibiting remarkable properties in slow-wave and highly sensitive sensing. In particular, tunable and ultracompact-chip-integrated EIT-like effects reveal fantastic application prospects in plasmonic circuits and networks. Here, we demonstrate an electrically tuned on-chip EIT analogue by means of dynamic EIT modules side-coupled to ultrathin corrugated metallic strips supporting spoof surface plasmon polaritons (SSPPs). By embedding PIN diodes into the subradiant mode, on-to-off control of the destructive coupling between the radiative and subradiant modes results in dynamic chip-scale EIT-like behavior under the change of the bias voltage, allowing for an electrically tunable group delay of the surface waves. The physical mechanism of the active modulation is elucidated with the coupled mode theory. In addition, the cascaded capacity performed by installing multiple EIT modules with an interval of equivalent wavelength are also characterized on a planar plasmonic waveguide. The proposed system will pave a versatile route toward dynamic control in chip-scale functional devices.

**Keywords:** electromagnetically induced transparency; spoof surface plasmon polariton; electrically control



**Citation:** Su, X.; Dong, L.; He, J.; Huang, Y.; Deng, F.; Liu, L.; Shi, Y.; Xu, Q.; Li, Y. Active Control of Electromagnetically Induced Transparency Analogy in Spoof Surface Plasmon Polariton Waveguide. *Photonics* **2022**, *9*, 833. <https://doi.org/10.3390/photonics9110833>

Received: 17 September 2022

Accepted: 3 November 2022

Published: 6 November 2022

**Publisher's Note:** MDPI stays neutral with regard to jurisdictional claims in published maps and institutional affiliations.



**Copyright:** © 2022 by the authors. Licensee MDPI, Basel, Switzerland. This article is an open access article distributed under the terms and conditions of the Creative Commons Attribution (CC BY) license (<https://creativecommons.org/licenses/by/4.0/>).

## 1. Introduction

Electromagnetically induced transparency (EIT) is a quantum destructive interference phenomenon that occurs between two different excitation pathways in a three-level atomic system, resulting in a narrow transparency window accompanied with sharp dispersion [1,2]. This unique characteristic has promising applications in such areas as optical data buffering [3], ultrafast switching [4], and biochemical sensing [5]. As a remarkable feature of the EIT spectral response, the slow-wave effect has a profound impact on electromagnetic science and communication technology [6–8]. Owing to rigorous implementation conditions, analogous EIT effects have been explored instead by near-field coupling between bright (radiative) and dark (subradiant) elements in coupled classical resonator systems [9–13]. Furthermore, various tunable media have been embedded into the resonators to obtain a dynamic response of the EIT-like effects, such as graphene [14–16], photosensitive elements [17,18], microelectromechanical systems [19], and phase change materials [20]. However, these configurations cannot be applied in practical integrated photonic circuits because the plasmonic structures need to be illuminated by input waves perpendicular to the upper plane [21]. An analogous EIT behavior performed directly in planar plasmonic structures is of particular interest for integration with versatile on-chip functionalities. Although phase-coupled mechanisms [22] and coupled microcavity mechanisms [23,24] in conventional microstrip lines have been presented, the dynamic

control and cascaded arrangement of the EIT-like effect in a chip-scale framework remain a considerable challenge.

Surface plasmon polaritons (SPPs) form at the interface between two materials with opposite real parts of the permittivity at the operation wavelength, for instance, a metal–dielectric interface at optical frequencies [25,26]. Owing to their capabilities to overcome the classical diffraction limit, SPPs are regarded as one of the most promising platforms for the minimization of on-chip integrated devices. At lower frequencies (far infrared, terahertz, or microwave), metal surfaces decorated with periodic subwavelength grooves or holes can imitate the intriguing properties of conventional optical SPPs, thus giving birth to the concept of spoof surface plasmon polaritons (SSPPs) [27–29]. The dispersion characteristics of the textured metals can be readily controlled by the geometric configurations. As a result, SSPP waveguide structures have the advantages of easy fabrication, strong field confinement, and acceptable propagation length, and the related functional components have been developed from conceptual models to practical applications [30–35].

In this work, we report the realization of an electrically tuned on-chip EIT analogue by means of two EIT modules symmetrically side-coupled to a corrugated SSPP waveguide. As the building blocks, each EIT module combines two types of split-ring resonators (SRR), one passive SRR and one active SRR integrated with a PIN diode. By applying a bias voltage to the PIN diodes, near-field coupling in the hybrid waveguide system enables dynamic modulation, achieving on-to-off control of the EIT-like behavior in the SSPP waveguide. Both full-wave simulations and theoretical calculations are in good agreement with experimental characterizations, and the mechanism of the active modulation is attributed to a shift in the resonance frequency of the active SRR caused by the variable capacitance once the bias voltage switches on. Furthermore, the tunable capacity of the EIT-effect and group delay in a cascaded arrangement are also investigated. The proposed scheme would open up the possibility of achieving ultracompact and reconfigurable plasmonic components in highly integrated circuits and networks.

## 2. Structure and Simulation

It is worthwhile to note that the ultrathin conformal SSPP scheme is a powerful route for microwave and terahertz plasmonic circuits due to its flexibility, low-loss, and broadband features [29]. As shown in Figure 1a, the corrugated SSPP waveguide is constructed by arranging two-sided metallic strips as the unit cells along the  $x$ -axis periodically, in which the groove width and groove depth are denoted as  $a$  and  $h$ , and the strip height and thickness are indicated as  $H$  and  $t$ , respectively, with a period of  $p$ . The metallic structure is placed on a 0.5 mm-thick ( $d$ ) dielectric substrate (F4B) with a relative permittivity of 2.65 and loss tangent of 0.002. By using the eigenmode solver of full-wave simulation, the dispersion curves of the SSPP waveguide with different groove depths  $h$  are constructed and are presented in Figure 1a, where the other geometrical parameters are chosen as  $p = 5$  mm,  $a = 2$  mm,  $t = 0.018$  mm, and  $H = 8$  mm. It can be seen that the dispersion curves are deviating gradually from the light line and asymptotically approaching different cutoff frequencies as the groove depth increases, and the corresponding coverage of the evanescent field provided by the corrugated strips is restricted drastically. The groove depth  $h$  is set to 3 mm to obtain a tradeoff between tight SSPP confinement and near-field interaction between corrugated strips and adjacent meta-particles. In order to launch SSPPs efficiently, a conversion structure (II) with  $50 \Omega$  impedance consisting of gradient corrugation grooves and a flaring ground are employed to connect the co-planar waveguide (I) and spoof SPP waveguide (III), as shown in the inset of Figure 1b. The exponential equation of the flaring ground is given as:  $y = w(e^{\alpha x} - 1) / (e^{\alpha l} - 1)$ , where  $\alpha = 0.14$  is defined as the exponential factor of the curve, and the width ( $w$ ) and length ( $l$ ) of the transition section are set as 25 mm and 60 mm, respectively. The simulated  $S$ -parameters are shown in Figure 1b, where the left (right) side of the hybrid waveguides is defined as Port 1 (2). It can be seen that the transmission coefficient ( $S_{21}$ ) is larger than  $-3$  dB, and the reflection coefficient ( $S_{11}$ ) is lower than  $-17$  dB within the passband range from 1.1 GHz to 12.8 GHz, indicating the

excellent impedance matching from the guide wave on the coplanar structure to the SSPPs on the two-sided metallic strips. Figure 1c,d illustrate, respectively, the simulated near-field distribution of the entire scheme and the partially enlarged sketch of the evanescent field vectors produced by the metallic grooves in the  $x$ - $y$  plane at an arbitrary frequency of 6.01 GHz within the passband. It is clearly observed that the electric field arrows primarily orient toward the  $y$  direction and decay exponentially around the corrugated structure.

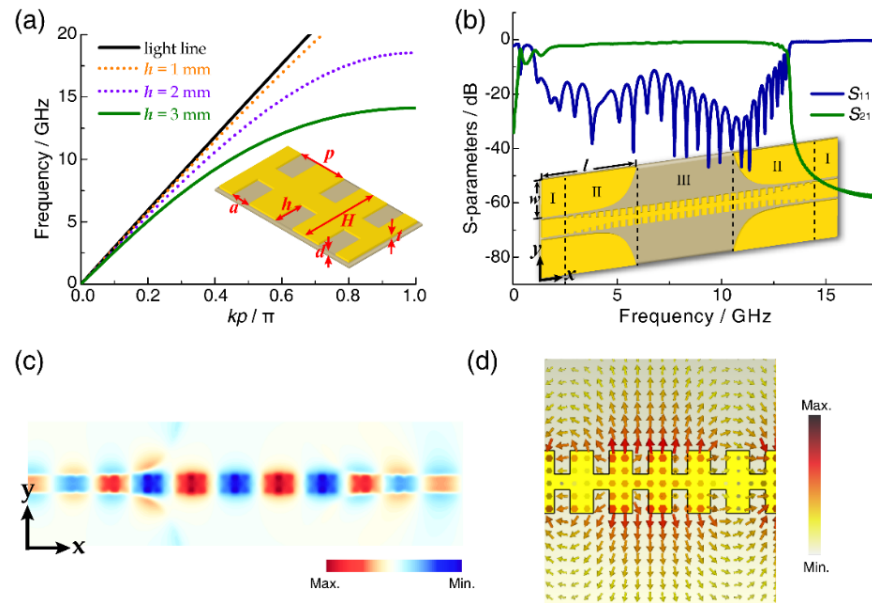


**Figure 1.** Prototype design and characteristics of SSPP waveguide based on two-sided metallic strips. (a) Dispersion curves have varying groove depths  $h$ , and the other geometrical parameters are fixed:  $p = 5$  mm,  $a = 2$  mm,  $H = 8$  mm,  $t = 0.018$  mm, and  $d = 0.5$  mm. (b) Transmission ( $S_{21}$ ) and reflection coefficients ( $S_{11}$ ) of SSPP waveguide, whose entire structure is shown in the inset. (c) Simulated electric field distribution at 6.01 GHz in the  $x$ - $y$  plane at 1.5 mm above the structure. (d) Electric field vectors of partial SSPP waveguide structure in the  $x$ - $y$  plane. The color scales of the arrows indicate the field amplitudes.

In the proposed tunable EIT-like configuration based on the SSPP waveguide, two sole EIT modules are symmetrically loaded in the close proximity of the two-sided metallic strips with a distance  $s_1 = 0.5$  mm, as illustrated in Figure 2a. An EIT module is constructed by an adjacent passive SRR and a remote active SRR, in which the structural parameters are set as: edge length  $p_x = p_y = 6$  mm, width  $w = 0.75$  mm,  $g_1 = 0.4$  mm,  $g_2 = 1$  mm, and  $s_2 = 0.5$  mm. Specifically, in each EIT module a PIN diode is mounted on the right-side gap between two nearby U-shaped rings to assemble an active SRR. As the top and bottom views of the sketch in Figure 2a show, two metallic through-holes are utilized to load a bias voltage from the bottom of the substrate. To eliminate the influence of the bias wires on the electromagnetic responses of the EIT-like system, three cascaded inductors with 100 nH are applied in each line to isolate the DC signal and radio frequency (RF) signal. Owing to the near-field distribution of the corrugated SSPP waveguide, the adjacent passive SRR in each EIT module can be excited strongly by the input wave and regarded as the radiative mode, whereas the remote active SRR could be excited only weakly and regarded as the subradiant mode. The ‘ON’ and ‘OFF’ states of the PIN diode tuned by the bias voltage determine the distinct resonance frequencies of the remote active SRR. In the full-wave simulation, the resistance ( $R_d$ ), inductance ( $L_d$ ), and capacitance ( $C_d$ ) of the PIN diode at the right gap of the active SRR in each EIT module are varied to imitate the effect of the ‘ON’ and ‘OFF’ states under the bias voltage (‘ON’ state:  $R_d = 0.9$   $\Omega$ ,  $L_d = 1.5$  nH; ‘OFF’ state:  $C_d = 0.3$  pF,  $L_d = 1.5$  nH). By optimizing the geometric parameters, the resonance frequencies of the subradiant mode in the ‘ON’ state and the radiative mode are nearly identical with a small

deviation, as illustrated in Figure 2b. Therefore, the EIT-like phenomenon can be achieved on the basis of the radiative–subradiant coupling mechanism and the transparency peak can be tuned through switching of the PIN diode integrated within the active SRR in each module. Figure 2c describes the on-to-off EIT-like peak modulation of the SSPP waveguide, achieving an amplitude modulation ratio of approximately 14 dB at 5.42 GHz.

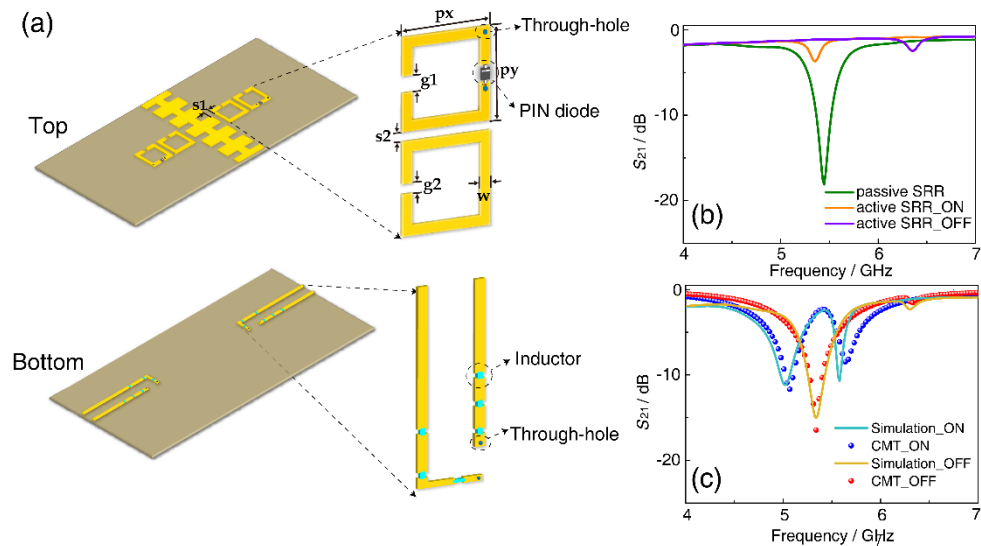


**Figure 2.** Schematic diagram and EIT-like transmission characteristics based on SSPP waveguide. (a) Top and bottom views of the proposed configuration, where the yellow part is metal and the brown part is dielectric substrate. (b) Transmission coefficients ( $S_{21}$ ) of SSPP waveguide loaded with single set of passive SRRs and active SRRs when the PIN diodes are in the ‘ON’ and ‘OFF’ states, respectively. (c) Simulated and theoretically fitted transmission coefficients ( $S_{21}$ ) of SSPP waveguide loaded with single set of EIT modules when the PIN diodes are in the ‘ON’ and ‘OFF’ states.

To explore the physical mechanism of the active modulation on the EIT-like effect in our proposed SSPP waveguide system, the widely used coupled-mode theory (CMT) model is employed to elucidate the near-field interaction between the combined SRR units and corrugated metallic strips [36]. According to the CMT, the resonance amplitudes of the radiative and subradiant modes are represented as  $a_1$  and  $a_2$  and can be expressed as:

$$\frac{\partial}{\partial t} \begin{pmatrix} a_1 \\ a_2 \end{pmatrix} = \left[ i \begin{pmatrix} \omega_1 & \kappa \\ \kappa & \omega_2 \end{pmatrix} - \begin{pmatrix} \gamma_1^s + \Gamma_1^i & 0 \\ 0 & \gamma_2^s + \Gamma_2^i \end{pmatrix} \right] \begin{pmatrix} a_1 \\ a_2 \end{pmatrix} + \begin{pmatrix} i\sqrt{\gamma_1^s} & 0 \\ 0 & 0 \end{pmatrix} \begin{pmatrix} S_{1+} \\ 0 \end{pmatrix} \quad (1)$$

where  $\omega_1$  and  $\omega_2$  are the center frequencies of the two resonant modes, respectively. The decay rate of each resonant mode includes two contributions, radiative damping  $\gamma_{1,2}^s$  and intrinsic damping  $\Gamma_{1,2}^i$ , and  $\kappa$  represents the coupling coefficient between these two resonances. The integrated system is fed only by the incoming wave from Port 1, denoted as  $S_{1+}$ . Moreover, the subradiant mode couples weakly with the incoming wave, which can be neglected. Hence, the transmission amplitude can be expressed as follows:

$$S_{21} = \frac{\kappa^2 + (i\omega - i\omega_1 + \Gamma_1^i) \cdot (i\omega - i\omega_2 + \gamma_2^s + \Gamma_2^i)}{\kappa^2 + (i\omega - i\omega_1 + \gamma_1^s + \Gamma_1^i) \cdot (i\omega - i\omega_2 + \gamma_2^s + \Gamma_2^i)} \quad (2)$$

By fitting  $S_{21}$  to the simulated transmission coefficients for the on and off states of the EIT-like phenomenon, the fitting results (spheres) are in good agreement with the full-wave simulations (solid curves) in Figure 2c, verifying the validity of the theoretical model. The fitting parameters are presented in Table 1.

**Table 1.** Fitting parameters based on CMT.

State	$\omega_1$	$\omega_2$	$\gamma_1^s$	$\gamma_2^s$	$\Gamma_1^i$	$\Gamma_2^i$	$\kappa$
ON	5.33	5.43	0.81	0.052	0.017	0.020	0.28
OFF	5.33	6.29	0.75	0.035	0.015	0.018	0.07

It is observed that the fitting resonance frequencies  $\omega_1$  and  $\omega_2$  are consistent with the transmission dips of the sole radiative mode and sole subradiant mode at the ‘ON’ and ‘OFF’ state of PIN diodes. The decay rate of each passive SRR is much stronger than that of each active SRR, particularly radiative damping  $\gamma_1^s$ , accounting for the major portion. Hence, the transmission feature of the SSPP waveguide is determined mainly by the reflection not the absorption. When each PIN diode is in the ‘ON’ state, the coupling coefficient  $\kappa$  is sufficiently large so that destructive interference occurred between radiative mode and subradiant mode results in the EIT-like response. On the contrary, in the ‘OFF’ state of the PIN diodes, the blueshift in the frequency of each active SRR from 5.43 GHz to 6.29 GHz contributes to a dramatic attenuation of the near-field coupling between radiative and subradiant modes and a slight suppression of the radiative damping  $\gamma_1^s$ , thus leading to disappearance of the EIT-like phenomenon and rejection of SSPP energy flow in the waveguide system. Therefore, it can be concluded that the dynamic modulation of the SSPP EIT-like behavior arises from a change in the coupling strength of the two resonant modes.

The on-to-off tunable EIT-like phenomenon in the SSPP waveguide can also be understood by analyzing the near electric-field distributions at the EIT peak frequency of 5.42 GHz. Figure 3 shows the normalized  $E_z$ -field distributions in the  $x$ - $y$  plane at 1.5 mm above the structure surface in the ‘ON’ and ‘OFF’ states, corresponding to pronounced EIT-like behavior appearance and EIT-like behavior disappearance in the SSPP waveguide system, respectively. According to the RLC circuit model of each active SRR, the electric resonance frequency is described by  $\omega_2 = (LC)^{-1/2}$ , where  $1/C = (1/C_g + 1/C_d)$ , with  $C_g$  being the gap capacitance of the left side,  $C_d$  the capacitance of each PIN diode, and  $L$  the total inductance. When each PIN diode is in the ‘ON’ state, it is clearly observed that the electric field is focused primarily around the remote active SRR gaps, whereas the electric field in the adjacent passive SRRs is completely suppressed in Figure 3a, which is the characteristic of typical EIT behavior. When the PIN diodes switch from the ‘ON’ state to the ‘OFF’ state, the resonance frequency shifts from 5.43 GHz to 6.29 GHz. Owing to a blueshift in resonance of each active SRR, the degradation in radiative–subradiant coupling results in the electric field being localized in the adjacent passive SRRs, as shown in Figure 3b. This reveals that switching of the PIN diodes alters the capacitance  $C_d$  of each active SRR, further manipulates the resonance frequency  $\omega_2$ , and has an impact on the destructive coupling between each passive SRR and active SRR, which eventually dominates the EIT-like transmission feature of the SSPP waveguide.

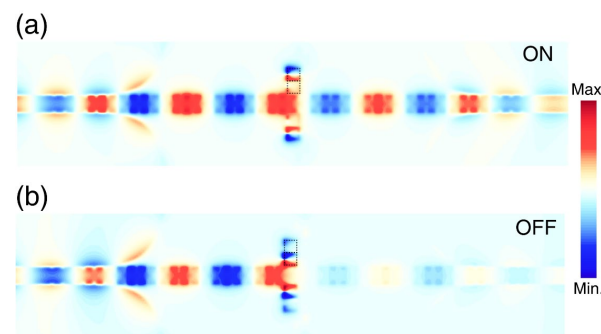


**Figure 3.** Simulated near-electric-field distributions in the  $x$ - $y$  plane at 1.5 mm above the entire structure at the EIT-like peak frequency of 5.42 GHz. The PIN diodes are in (a) ‘ON’ state ( $R_d = 0.9 \Omega$ ,  $L_d = 1.5$  nH), and (b) ‘OFF’ state ( $C_d = 0.3$  pF,  $L_d = 1.5$  nH), respectively. The dotted regions near the SSPP waveguide mark the locations of passive SRR and active SRR, respectively.

### 3. Measurement and Discussion

To perform experimental verification of the aforementioned functions, samples of a corrugated SSPP waveguide loaded with a single set of passive SRRs, active SRRs, and EIT modules were fabricated using the standard printed circuit board (PCB) technology, as shown in Figure 4a,c. The PCB fabrication is the process of transcribing a design pattern onto the physical structure of the copper laminate. The fabrication of our sample was divided into four steps, where the specific processes were cutting the double-sided copper laminate, drilling holes, pattern transferring (film formation, exposure, and development), and welding the PIN diodes, inductors, and SMA adapters. The geometric parameters used were the same as those in the above simulations, and the size of the entire sample was  $260\text{ mm} \times 58.5\text{ mm} \times 0.5\text{ mm}$ . In the measurements, the two endpoints of each sample were melded via SMA connectors and connected to a vector networks analyzer (N5230C, Agilent) through two coaxial cables with  $50\ \Omega$  port impedance. By applying a bias voltage to the PIN diodes (SMP1320-011, Skyworks) through metallic through-holes connected to two pieces of the bottom substrate, the capacitance of each active SRR could be modulated dynamically. When the forward voltage was changed from 0.85 V to 0 V, the states of the PIN diodes were switched between the ‘ON’ and ‘OFF’ states. Figure 4b,d display the measured transmission coefficients ( $S_{21}$ ) of each sample. It should be noted that the resonance responses of the samples with a single set of active SRRs and EIT modules in the ‘ON’ and ‘OFF’ states were relatively faint compared with those in simulations, likely caused by a larger resistance of the PIN diodes and higher loss in the actual dielectric substrate. Despite these discrepancies, the measured results confirm the tunable EIT-like phenomenon in the SSPP waveguide, where the destructive coupling between the radiative and subradiant modes depends on the dynamic resonance frequency detuning controlled by the bias voltage.

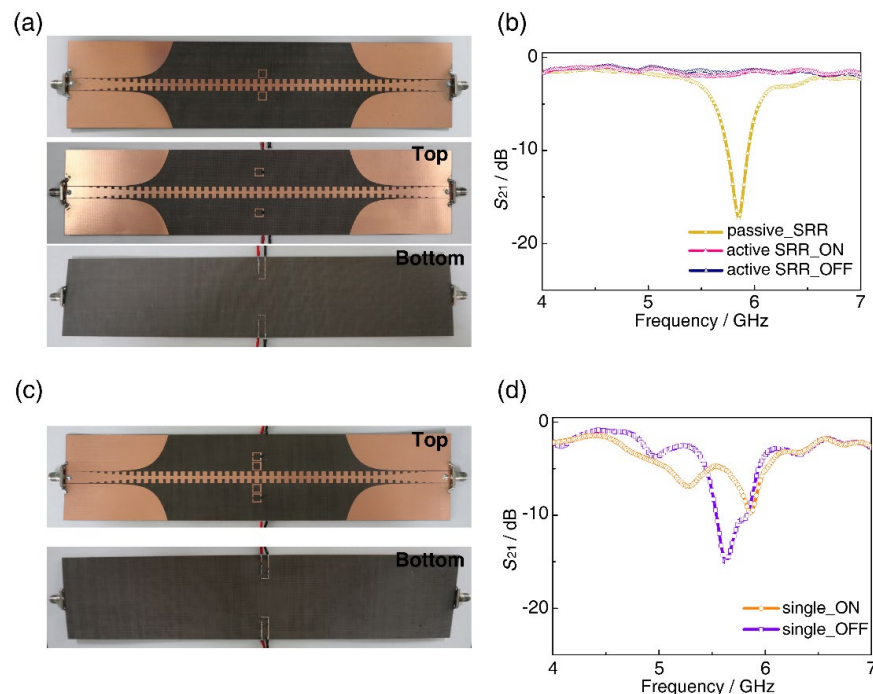


**Figure 4.** Experimental measurements of tunable EIT-like behavior in SSPP waveguide. (a) Photograph of fabricated SSPP waveguide samples loaded with single set of passive SRRs and active SRRs in top and bottom views. (b) Transmission coefficients corresponding to structures in (a). (c) Photograph of fabricated SSPP waveguide sample loaded with single set of EIT modules in top and bottom views. (d) Transmission coefficients corresponding to structures in (d). The word in Figure (a,c) indicates the top and bottom views, respectively.

In addition, a triple set of EIT modules were cascaded along the SSPP-propagating trajectory in a close vicinity of the corrugated strips, as illustrated in Figure 5a. According to the dispersion relation of the SSPP waveguide, the distance between each set of EIT modules was configured to be the operation wavelength  $\lambda_{sp} = 40$  mm of the EIT-like behavior, thus promoting the coherent accumulation in the waveguide system. As expected, when the forward voltage reached the threshold of the PIN diodes, the EIT-like response was activated and the SSPPs achieved high transmission at the working frequency. When no bias voltage or a reverse voltage was applied, the EIT-like response vanished and contributed to the rejection of SSPP propagation, with a modulation contrast of up to 19 dB at 5.42 GHz.

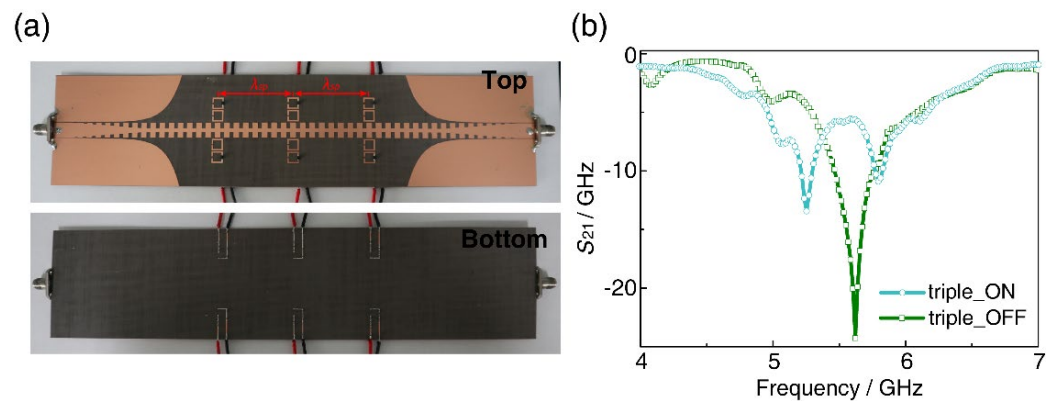


**Figure 5.** Experimental measurements of sample with three-cascaded EIT modules side-coupled to SSPP waveguide. (a) Photograph of fabricated sample in top and bottom views, and (b) corresponding transmission coefficients in ‘ON’ and ‘OFF’ states of PIN diodes. The word in Figure (a) indicates the top and bottom views, respectively.

Accompanying the occurrence of the EIT-like behavior, the dramatic change of the transmission phase within the transparency window resulted in a significant decrease of the SSPP group velocity, giving rise to the slow-wave effect on the chip that was described by the group delay. The use of group delay was more relevant to the transmission phase and given by  $t_g = \frac{d\varphi}{d\omega}$ , where  $\varphi$  and  $\omega$  are the transmission phase shift and angular frequency, respectively. The difference in the group delays that the SSPPs pass through the waveguide structure loaded with EIT modules in comparison with a pure waveguide structure of the same length can be retrieved from the derivative of the transmission phase with respect to frequency. Figure 6 illustrates the simulated transmission phases and calculated group delays of the SSPP waveguide samples loaded with single and triple sets of EIT modules when the PIN diodes were in the ‘ON’ and ‘OFF’ states. It can be seen that the SSPPs at the operation frequency 5.42 GHz were delayed by 0.53 ns and 1.36 ns when single and triple sets of EIT modules were in the working condition, respectively, which is equivalent to time delays of 22.87 mm and 58.68 mm in terms of distance in the pure waveguide structure.

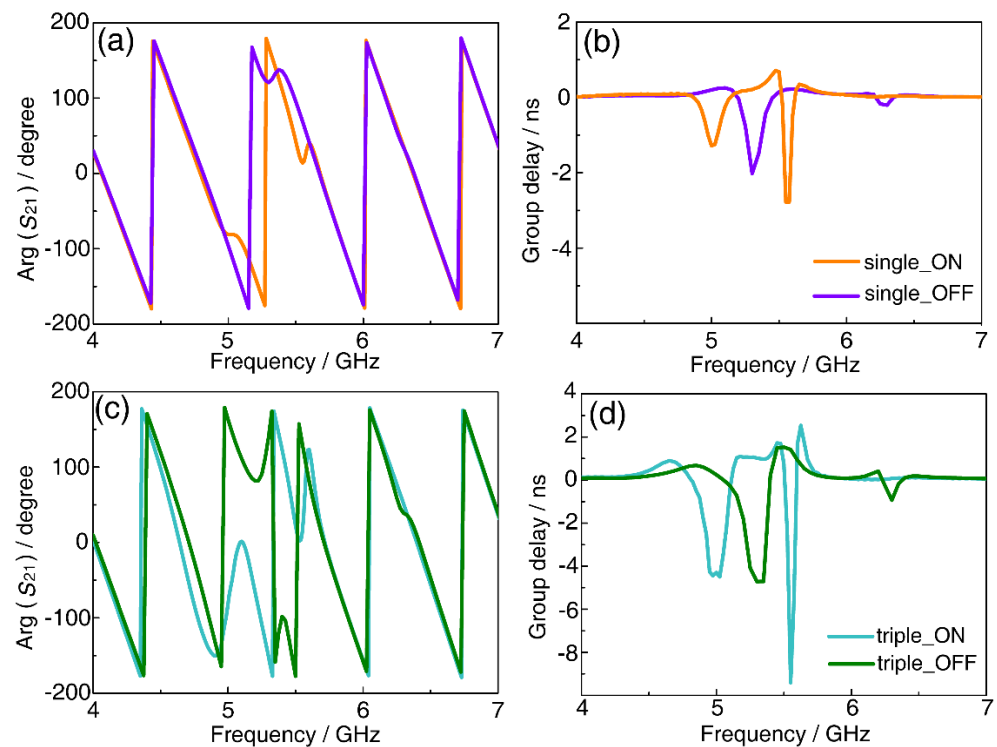


**Figure 6.** Transmission phases (a,c) and calculated group delays (b,d) of SSPP waveguide samples loaded with single and triple sets of EIT modules, when the PIN diodes are in the ‘ON’ and ‘OFF’ states.

#### 4. Conclusions

In summary, an on-to-off control of the EIT-like effect based on a corrugated SSPP waveguide is demonstrated by virtue of active EIT modules integrated with electrically controlled PIN diodes. As the bias voltage switches from 0.85 V (‘ON’ state) to 0 V (‘OFF’ state), the SSPP EIT-like transmittance experiences a drastic change due to the tunable destructive coupling between the combined SRR units. According to full-wave simulations, CMT analysis, and microwave measurements, the dynamic modulation is attributed to the suppression of the near-field coupling between the radiative and subradiant modes. Furthermore, tunable group delays are achieved in a cascaded arrangement by switching the bias voltage control. The proposed scheme not only introduces a new approach to design active on-chip EIT-like effects, but also constitutes an important step towards the realization of subwavelength integrated plasmonic circuits.

**Author Contributions:** Conceptualization, X.S. and Q.X.; methodology, X.S.; software, J.H.; validation, X.S., L.D., and Q.X.; formal analysis, F.D.; investigation, Y.H.; resources, Y.S.; data curation, L.L.; writing—original draft preparation, X.S.; writing—review and editing, Y.L.; supervision, Y.L.; funding acquisition, L.D. and Y.S. All authors have read and agreed to the published version of the manuscript.

**Funding:** This research was funded by National Natural Science Foundation of China (Grant No. 11874245, 62135008, 62005193, 61935015); The Central Government Guides Local Science and Technology Development Fund Projects (Grant No. YDZJSX2021B011); China Scholarship Council (Grant No. 202108140067); Scientific and Technological Innovation Programs of Higher Education Institutions in Shanxi (Grant No. 2021L369); and Yungang Special Fund of Shanxi Datong University (Grant No. 2020YGZX005).

**Institutional Review Board Statement:** Not applicable.

**Informed Consent Statement:** Not applicable.

**Data Availability Statement:** The data presented in this study are available on request from the corresponding author.

**Conflicts of Interest:** The authors declare no conflict of interest. The funders had no role in the design of the study; in the collection, analyses, or interpretation of data; in the writing of the manuscript; or in the decision to publish the results.

## References

1. Harris, S.E. Electromagnetically induced transparency. *Phys. Today* **1997**, *50*, 36–42. [[CrossRef](#)]
2. Fleischhauer, M.; Imamoglu, A.; Marangos, J.P. Electromagnetically induced transparency: Optics in coherent media. *Rev. Mod. Phys.* **2005**, *77*, 633. [[CrossRef](#)]
3. Phillips, D.F.; Fleischhauer, A.; Mair, A.; Walsworth, R.L.; Lukin, M.D. Storage of light in atomic vapor. *Phys. Rev. Lett.* **2001**, *86*, 783. [[CrossRef](#)] [[PubMed](#)]
4. Manzacca, G.; Cincotti, G.; Hingerl, K. Ultrafast switching by controlling Rabi splitting. *Appl. Phys. Lett.* **2007**, *91*, 231920. [[CrossRef](#)]
5. Zhang, J.; Mu, N.; Liu, L.H.; Xie, J.H.; Feng, H.; Yao, J.Q.; Chen, T.; Zhu, W.R. Highly sensitive detection of malignant glioma cells using metamaterial-inspired THz biosensor based on electromagnetically induced transparency. *Biosens. Bioelectron.* **2021**, *185*, 113241. [[CrossRef](#)]
6. Lee, M.J.; Ruseckas, J.; Lee, C.Y.; Kudriasov, V.; Chang, K.F.; Cho, H.W.; Juzeliūnas, G.; Yu, I.A. Experimental demonstration of spinor slow light. *Nat. Commun.* **2014**, *5*, 5542. [[CrossRef](#)]
7. Lukin, M.D.; Imamoglu, A. Controlling photons using electromagnetically induced transparency. *Nature* **2001**, *413*, 273–276. [[CrossRef](#)]
8. Xiao, B.; Wang, Y.; Cai, W.; Xiao, L. Design and prediction of PIT devices through deep learning. *Opt. Express* **2022**, *30*, 14985–14997. [[CrossRef](#)]
9. Xu, Q.; Sandhu, S.; Povinelli, M.L.; Shakya, J.; Fan, S.; Lipson, M. Experimental realization of an on-chip all-optical analogue to electromagnetically induced transparency. *Phys. Rev. Lett.* **2006**, *96*, 123901. [[CrossRef](#)]
10. Zhang, Z.R.; Zhang, L.W.; Li, H.Q.; Chen, H. Plasmon induced transparency in a surface plasmon polariton waveguide with a comb line slot and rectangle cavity. *Appl. Phys. Lett.* **2014**, *104*, 231114. [[CrossRef](#)]
11. Zhang, S.; Genov, D.A.; Wang, Y.; Liu, M.; Zhang, X. Plasmon-induced transparency in metamaterials. *Phys. Rev. Lett.* **2008**, *101*, 047401. [[CrossRef](#)]
12. Papasimakis, N.; Fedotov, V.A.; Zheludev, N.I.; Prosvirnin, S.L. Metamaterial analog of electromagnetically induced transparency. *Phys. Rev. Lett.* **2008**, *101*, 253903. [[CrossRef](#)]
13. Singh, R.; Plum, E.; Menzel, C.; Rockstuhl, C.; Azad, A.K.; Cheville, R.A.; Lederer, F.; Zhang, W.; Zheludev, N.I. Terahertz metamaterial with asymmetric transmission. *Phys. Rev. B* **2009**, *80*, 153104. [[CrossRef](#)]
14. Zhang, J.; Li, Z.; Shao, L.; Xiao, F.; Zhu, W. Active modulation of electromagnetically induced transparency analog in graphene-based microwave metamaterial. *Carbon* **2021**, *183*, 850–857. [[CrossRef](#)]
15. Cai, W.; Xiao, B.; Yu, J.; Xiao, L. A compact graphene metamaterial based on electromagnetically induced transparency effect. *Opt. Commun.* **2020**, *475*, 126266. [[CrossRef](#)]
16. Xiao, B.; Zhu, J.; Xiao, L. Tunable plasmon-induced transparency in graphene metamaterials with ring–semiring pair coupling structures. *Appl. Opt.* **2020**, *59*, 6041–6045. [[CrossRef](#)]
17. Liu, K.; Lian, M.; Qin, K.; Zhang, S.; Cao, T. Active tuning of electromagnetically induced transparency from chalcogenide-only metasurface. *Light Adv. Manuf.* **2021**, *2*, 1. [[CrossRef](#)]
18. Dhama, R.; Panahpour, A.; Pihlava, T.; Ghindani, D.; Caglayan, H. All-optical switching based on plasmon-induced Enhancement of Index of Refraction. *Nat. Commun.* **2022**, *13*, 1–9. [[CrossRef](#)]
19. Manjappa, M.; Pitchappa, P.; Singh, N.; Wang, N.; Zheludev, N.I.; Lee, C.; Singh, R. Reconfigurable MEMS Fano metasurfaces with multiple-input–output states for logic operations at terahertz frequencies. *Nat. Commun.* **2018**, *9*, 4056. [[CrossRef](#)]
20. Jeong, Y.G.; Bahk, Y.M.; Kim, D.S. Dynamic terahertz plasmonics enabled by phase-change materials. *Adv. Opt. Mater.* **2020**, *8*, 1900548. [[CrossRef](#)]
21. Xia, S.; Zhai, X.; Wang, L.; Xiang, Y.; Wen, S. Plasmonically induced transparency in phase-coupled graphene nanoribbons. *Phys. Rev. B* **2022**, *106*, 075401. [[CrossRef](#)]
22. Kekatpure, R.D.; Barnard, E.S.; Cai, W.; Brongersma, M.L. Phase-coupled plasmon induced transparency. *Phys. Rev. Lett.* **2010**, *104*, 243902. [[CrossRef](#)] [[PubMed](#)]
23. Chai, Z.; Hu, X.Y.; Zhu, Y.; Sun, S.B.; Yang, H.; Gong, Q.H. Ultracompact chip-integrated electromagnetically induced transparency in a single plasmonic composite nanocavity. *Adv. Opt. Mater.* **2014**, *2*, 320–325. [[CrossRef](#)]
24. Hu, Y.; Liu, W.; Sun, Y.; Shi, X.; Jiang, J.; Yang, Y.; Zhu, S.; Evers, J.; Chen, H. Electromagnetically-induced-transparency-like phenomenon with resonant meta-atoms in a cavity. *Phys. Rev. A* **2015**, *92*, 053824. [[CrossRef](#)]
25. Berini, P.; De Leon, I. Surface plasmon polariton amplifiers and lasers. *Nat. Photonics* **2021**, *6*, 16–24. [[CrossRef](#)]
26. Min, B.; Ostby, E.; Sorger, V.; Ulin-Avila, E.; Yang, L.; Zhang, X.; Vahala, K. High-Q surface-plasmon-polariton whispering-gallery microcavity. *Nature* **2009**, *457*, 455–458. [[CrossRef](#)]
27. Pendry, J.B.; Martín-Moreno, L.; García-Vidal, F.J. Mimicking surface plasmons with structured surfaces. *Science* **2004**, *305*, 847–848. [[CrossRef](#)]

28. Garcia-Vidal, F.J.; Martín-Moreno, L.; Pendry, J.B. Surfaces with holes in them: New plasmonic metamaterials. *J. Opt. Pure Appl. Opt.* **2005**, *7*, 97–101. [[CrossRef](#)]
29. Shen, X.; Cui, T.J.; Martín-Cano, D.; Garcia-Vidal, F.J. Conformal surface plasmons propagating on ultrathin and flexible films. *Proc. Natl. Acad. Sci. USA* **2013**, *110*, 40–45. [[CrossRef](#)]
30. Tang, W.X.; Zhang, H.C.; Ma, H.F.; Jiang, W.X.; Cui, T.J. Concept, theory, design, and applications of spoof surface plasmon polaritons at microwave frequencies. *Adv. Opt. Mater.* **2019**, *7*, 1800421. [[CrossRef](#)]
31. Su, X.; Xu, Q.; Lu, Y.; Zhang, Z.; Xu, Y.; Zhang, X.; Li, Y.; Ouyang, C.; Deng, F.; Liu, Y.; et al. Gradient Index Devices for Terahertz Spoof Surface Plasmon Polaritons. *ACS Photonics* **2020**, *7*, 3305–3312. [[CrossRef](#)]
32. Gao, Z.; Wu, L.; Gao, F.; Luo, Y.; Zhang, B. Spoof plasmonics: From metamaterial concept to topological description. *Adv. Mater.* **2018**, *30*, 1706683. [[CrossRef](#)]
33. Zhang, X.; Xu, Q.; Xia, L.; Li, Y.; Gu, J.; Tian, Z.; Ouyang, C.; Han, J.; Zhang, W. Terahertz surface plasmonic waves: A review. *Adv. Photonics* **2020**, *2*, 1–19. [[CrossRef](#)]
34. Zhang, L.; Zhang, H.; Tang, M.; He, P.; Niu, L.; Liu, L.; Lu, J.; Tang, W.; Mao, J.; Cui, T. Integrated multi-scheme digital modulations of spoof surface plasmon polaritons. *Sci. China Inf. Sci.* **2020**, *63*, 202302. [[CrossRef](#)]
35. Zhang, H.C.; Cui, T.J.; Luo, Y.; Zhang, J.; Xu, J.; He, P.H.; Zhang, L.P. Active digital spoof plasmonics. *Natl. Sci. Rev.* **2020**, *7*, 261–269. [[CrossRef](#)]
36. Fan, S.; Suh, W.; Joannopoulos, J.D. Temporal coupled-mode theory for the Fano resonance in optical resonators. *J. Opt. Soc. Am. A* **2003**, *20*, 569–572. [[CrossRef](#)]